On-Surface Synthesis: A New Route Realizing Single-Layer Conjugated Metal–Organic Structures

Jing Liu, Mathieu Abel, Nian Lin

On-surface Synthesis: A New Route Realizing Single-Layer Conjugated Metal-Organic Structures

Jing Liu[1], Mathieu Abel[2] and Nian Lin[3]

[1]Division of Quantum State of Matter, Beijing Academy of Quantum Information Sciences, 100193 Beijing, China

[2]Aix Marseille Univ, CNRS, IM2NP, Marseille,13397, France

[3]Department of Physics, The Hong Kong University of Science and Technology, Clear Water Bay, Hong Kong, China

Abstract

Recently, both experimental and theoretical advances have demonstrated that two-dimensional conjugated metal-organic frameworks (2D-cMOFs) exhibit interesting electronic and magnetic properties, such as high conductivity and ferromagnetism. Theoretical studies have predicted that exotic quantum states, including topological insulating states and superconductivity, emerge in some 2D-MOFs. The high design tunability of MOFs' structure and composition provides great opportunities to realize these structures. However, most of conventional synthesis methods yield multi-layer structures of the 2D-cMOFs, in which the predicted exotic quantum phases are often quenched due to inter-layer interactions. It is highly desirable to synthesize single-layer cMOFs.

On-surface synthesis represents a novel strategy towards this goal. In this Perspective, we discuss the recent developments in on-surface synthesis of 1D- and 2D-cMOFs.

Metal−organic frameworks (MOFs) represent a class of functional materials for wide range applications including gas and energy storage, filtration, catalysis, and sensing owing to their versatile structural and functional properties.[1-4] From the structure point of view, MOFs are considered crystals that comprise lattices of metal atoms and molecules. The structural and compositional tunability of MOFs provides an appealing playground for designing specific lattices. Majority of MOFs features poor electric conductivity because the coordination bonds normally feature weak electronic coupling which does not provide effective hopping between the neighboring sites. This problem can be overcome when coordination modes render aromaticity or quasi-aromaticity.[5] It has been found that a tetra-coordinated square-planar bis-(di-X)M coordination satisfies this requirement. As shown in Scheme 1, a metal ion M and two di-X ligands (X=thiol, hydroxyl, amino) constitute two inter-connected five-member rings. The electronic coupling between the π orbital of the di-X ligands and the d orbital of the metal ion delocalizes the π electrons over the two five-member rings, offering efficient π-conjugation, namely, quasi-aromaticity. This type of coordination yields so-called conjugated MOFs.[6] 2D-cMOFs represents a new family of 2D crystals that are uniquely different from inorganic 2D materials such as graphene or boron nitride which are not easily to be functionalized, or 2D organic polymers that are lack of good crystalline.

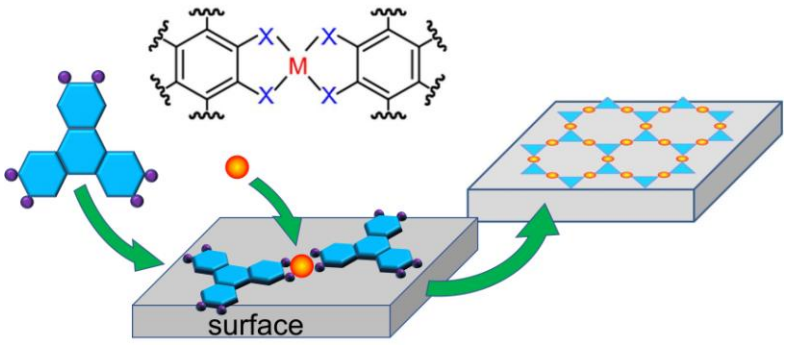

Scheme 1 On-surface synthesis of single-layer 2D-cMOFs based on bis-(di-X)M coordination (X=thiol, hydroxyl, amino).

Research on 2D-cMOFs prior to 2012 has been mostly focused on structural analysis rather than on their physical properties. Recently, more and more breakthroughs have been made reporting electrochemical activity, photoactivity, semiconductivity, high electrical conductivity and ferromagnetism in 2D-cMOFs.[7-15] Remarkably, conductivity of up to 1580 S cm^{-1} was obtained in the 15−500 nm thick films of a Cu-BHT MOF.[9] This high conductivity is attributed to the strong π−d interaction between the metal ions and ligands and to the delocalized electrons in the 2D system. More excitingly, this material was reported to be a single-layer superconductor.[16,17] Another interesting example is a 2D-cMOF exhibiting ferromagnetic ordering below ~20 K.[18]

Concurrent with these experimental advances, theoretical investigations have progressed rapidly. The work of Feng Liu's group, leading to the prediction of the existence of organic topological materials in a series of publications,[19-23] is an exciting development. The 2D-cMOFs with bis-(di-X)M coordination have received wide interest. For example, a bis(dithiolato)Mn 2D-MOF was predicted to be a ferromagnetic spin−lattice with S = 3/2.[24] The spins in the unit cell form long-range ferromagnetic ordering mediated by p−d hybridization resulting from the π-conjugated Kagome lattice. Octaaminonaphthalene-M (M=Fe, Cr, or Co) 2D-MOFs were reported to exhibit half-metallic nature resulting in remarkable 100% spin-filtering efficiency.[25] Hexaiminotriphenylene Ni or Cu (Ni-HATP or Cu-HATP) 2D-MOFs display metallic band structures. Zhou *et al*. showed that d^8 transition metals (Pt and Pd) induce spin orbit coupling (SOC) gaps and the gaps of the NH coordinated complexes are much larger than their amino counterparts.[27]

These predicted physical properties of the single-layer systems are often different in the multi-layer structures in which the inter-layer interactions in the stacked layers may quench the exotic quantum phases. It is thus highly desirable to synthesize single-layer 2D-cMOFs. However, traditional hydro-/solvothermal methods yield crystalline powders of 2D-cMOFs.[28] The interface-assisted synthesis methods, including gas-liquid and liquid-liquid interfacial synthesis, Langmuir-Blodgett (LB) method, solid-liquid interfacial synthesis, are used for synthesizing films and layers of 2D-cMOFs whose thickness ranges from 1−2 μm to 10 nm. To date, only one work reported by Feng's group successfully fabricated a single layer 2D-cMOF which features thickness of ~0.7 nm using the LB method.[29]

On-surface synthesis provides a unique approach for fabricating single-layer metal-organic structures. As illustrated in Scheme 1, the linker molecules functionalized with specific chemical groups and metal atoms are deposited on an atomic flat surface, and after annealing at an appropriate temperature, single-layer 2D-MOFs form on the surface. This method has yielded a large variety of 2D-MOFs comprising hexagonal, triangular, square, Kagome, or other complex lattices of metal atoms.[30] The whole process normally is conducted in ultra-high vacuum conditions, which enable the state-of-art microscopic and spectroscopic characterizations in further steps. In this perspective, we will discuss the recent progresses in the design, synthesis and characterization of single-layer 1D- and 2D-cMOF structures using the on-surface synthesis. We will exemplify several combined experimental and theoretical studies concerning (1) the electronic structures, and (2) the magnetic properties of the on-surface synthesized single-layer 1D- and 2D-cMOFs to highlight the advances in the field.

In recent years, on-surface synthesis has emerged as a remarkable strategy to create and isolate single layer of organized 1D-cMOF chains using the surface as a template to drive the

assembly and to catalyze the reactions. Benzene-based molecules have been used to react with metal atoms (Scheme 2). [31-38] All these molecules are based on a phenyl ring with four radicals: i) a zwitterionic quinone (ZQ) functionalized by 2 amine groups and two carboxylic groups, ii) tetrahydroxy benzene (THB) and iii) 2,5 diamino-1,4benzoquinonediimines (2HQDI). The formation of 1D-cMOFs from these molecules proceeds by successive deprotonation/metalation steps in which two covalent bonds and two coordinative bonds are formed between the metal center and two adjacent molecules. This provides a metal oxidation state +II and a full delocalization of the π electrons. The presence of metal centers regularly spaced in the conductive chain is very promising to introduce magnetic properties in the 1D-cMOF.

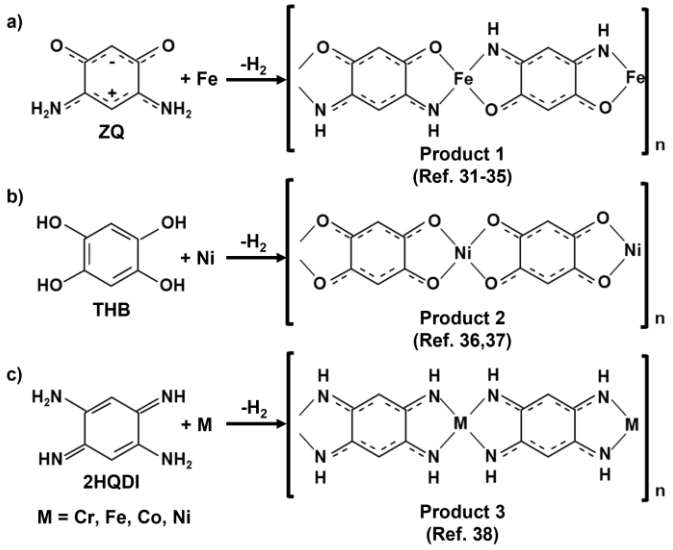

Scheme 2 Schematic illustration of the 1D coordination reactions used for the synthesis of 1D-cMOFs on surfaces. (a) 1D-cMOF obtained from ZQ and Fe atoms. (b) 1D-cMOF from THB and Ni atoms. (c) 1D-cMOF obtained from 2HQDI and different metals (M=Cr, Fe, Co, Ni).

Strictly 1D-cMOFs (nanowires) are fascinating from fundamental and applied points of views.[39] While non-covalent metal-organic coordination chains are well documented,[40-41] covalent links (*i.e.*, with preservation of conjugation) between metal and organic molecules to

form cMOFs have just emerged.[42-47] Due to the growth process used so far, the extension of these nanowires is often limited. To overcome this limitation, reactive growth process was used involving ZQ and iron atoms co-deposition on a Ag(111) substrate held at 200 °C (Figure 1a-d). The reaction proceeds by successive deprotonation/metalation steps and finally wires in which each quinoid unit is linked to the metal center by two covalent and two coordinative bonds through N and O atoms, thereby producing a π electrons delocalized over the entire 1D-cMOF. This is confirmed by X-ray photoelectron spectroscopy (XPS) experiments and allows the formation of micrometer size 1D-cMOF.[31] In this case the distance between two molecules is measured to be 7.6 Å in a (√7x √7) R20° superstructure. This lattice parameter is found very close to the equilibrium lattice parameter calculated by DFT when intermediate spin state is considered for each Fe atoms (S = 1). When this ZQ-Fe cMOF is deposited on Au(110), the lattice parameter is enlarged to 8.2 Å due to a c(4x2) epitaxial relationship measured by LEED (Figure 1e-h). Such a large lattice parameter comparing to the one obtained on Ag(111) (7.6 Å) cannot be interpreted without taking into account a spin crossover (SCO) phenomenon where the spin state of Fe atom change from S = 1 to S = 2 and the associated equilibrium lattice changes from 15.4 Å to 15.9 Å (*i.e.*, 7.7 Å and 7.95 Å between adjacent molecules) (Figure 1i).[31]

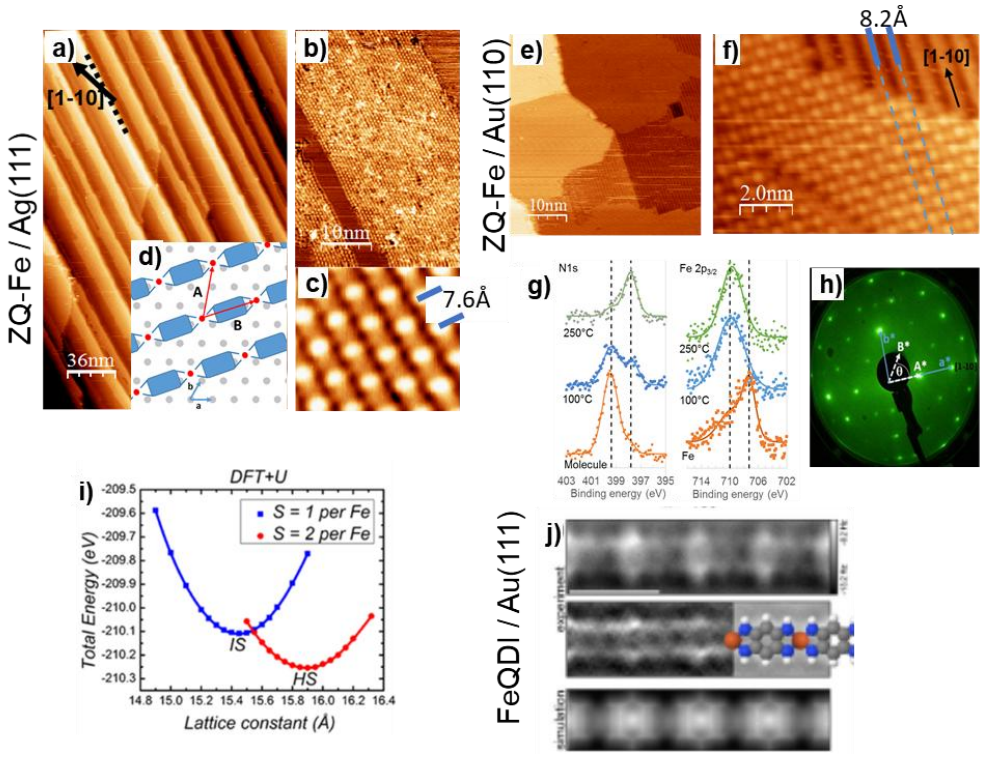

Figure 1 (a,b) STM images of ZQ co-deposited with Fe on Ag(111) with alignment of 1D chains of Product 1 with respect to step edges. (c) High resolution image. (d) Schematic model of the epitaxial relationship (√7x √7) R20°. Adapted with permission from Ref. 31. Copyright 2016 Springer-Nature. (e,f) STM images of ZQ co-deposited with Fe on Au(110). (g) N1s XPS spectra of pristine molecule, and its co-depostion with Fe atoms at 100°C and 250°C on Au(110) and Fe 2p3/2 XPS spectra of Fe/Au(110) molecule, and its co-depostion with ZQ molecules at 100 °C and 250 °C (h) LEED pattern of the c(4x2) superstructure. (i) DFT calculations of the lattice parameter of the free standing 1D chain (ZQ-Fe) with respect to the spin state of Fe atoms, *S*(Fe) = 1 for intermediate spin state and *S*(Fe) = 2 for high spin state (GGA+U). Adapted with permission from Ref.32. Copyright 2018 American Chemical Society. (j) High resolution constant height nc-AFM image (scale bar: 1nm) of Fe-QDI/Au(111) (top), filtered image (middle), AFM simulated image (bottom). Adapted with permission from Ref. 38. Copyright 2020 Wiley-VCH.

1D-cMOF (Product 3) comprising 2HQDI and metal atoms (M = Cr, Fe, Co, Ni) are formed on Au(111) and Cu(111).[38] A combination of XPS, STM, nc-AFM, and DFT calculations was used to characterize in (Figure 1j), demonstrating that all metal atoms adopt a fourfold coordination motif with the nitrogen atoms after dehydrogenation of the 2HQDI molecules providing a full delocalization of the π-d electron system over the entire 1D-cMOF. In contrast, complexation between Cu adatoms and 2HDQI molecules on Cu(111), a different configuration of the metal is obtained, in which 2-fold coordination of Cu atoms preventing the full delocalization of the electron density over the nanowire.[38]

Transition metal complexes with 4 to 7 d electrons can adopt different spin configurations either high-spin, intermediate-spin and low-spin depending on ligand field splitting, and SCO has been observed under external stimuli such as light, pressure temperature or electric field.[48] The on-surface synthesis of 1D-cMOF has allowed a description and manipulation of individual spin state at the atomic level. As presented above in the case of ZQ-Fe 1D-cMOF, the epitaxial relationship between the spin chain and the substrate can be used to strain the molecular wire forcing it to change spin state from $S = 1$ to $S = 2$ (Figure 2). This phenomena in 1D-cMOF chains of THB and Ni atoms synthesized on different Au substrates [Au(111), Au(110) and Au(100)] are studied using STM, STS under magnetic field and DFT calculations.[37] Distinct STM topographies of the 1D-cMOFs are observed on the three Au surfaces (Figure 2a).[37] On Au(100) [Au(110)], most Ni atoms in the chains are darker (brighter) than the molecular moieties, while on Au(111), darker and brighter Ni atoms arrange alternately along the chains. High resolution STS measurements reveal the different spin states of the brighter and darker Ni atoms. The dI/dV spectra acquired at the brighter Ni atoms on Au(110) and Au(111) feature zero-bias anomalies which are attributed to the Kondo resonance of the spin electrons localized on the

Ni atoms (Figure 2b). As a comparison, the darker Ni atoms on Au(100) and Au(111) show featureless spectra around the Fermi level, indicating the absence of Kondo effect. The experimental results are in accordance with the DFT calculations demonstrating an S = 1 (high spin, HS) state of the brighter Ni atoms on Au(110) and Au(111) while an S = 0 (low spin, LS) state of the darker Ni atoms on Au(100) and Au(111). Different spin-state phases of the 1D-cMOFs are identified on the three Au surfaces, that is, a LS phase on Au(100), a HS phase on Au(110), and an antiferroelastic (AFE) phase with alternately arranged HS- and LS-Ni atoms along the chains on Au(111) (Figure 2a).

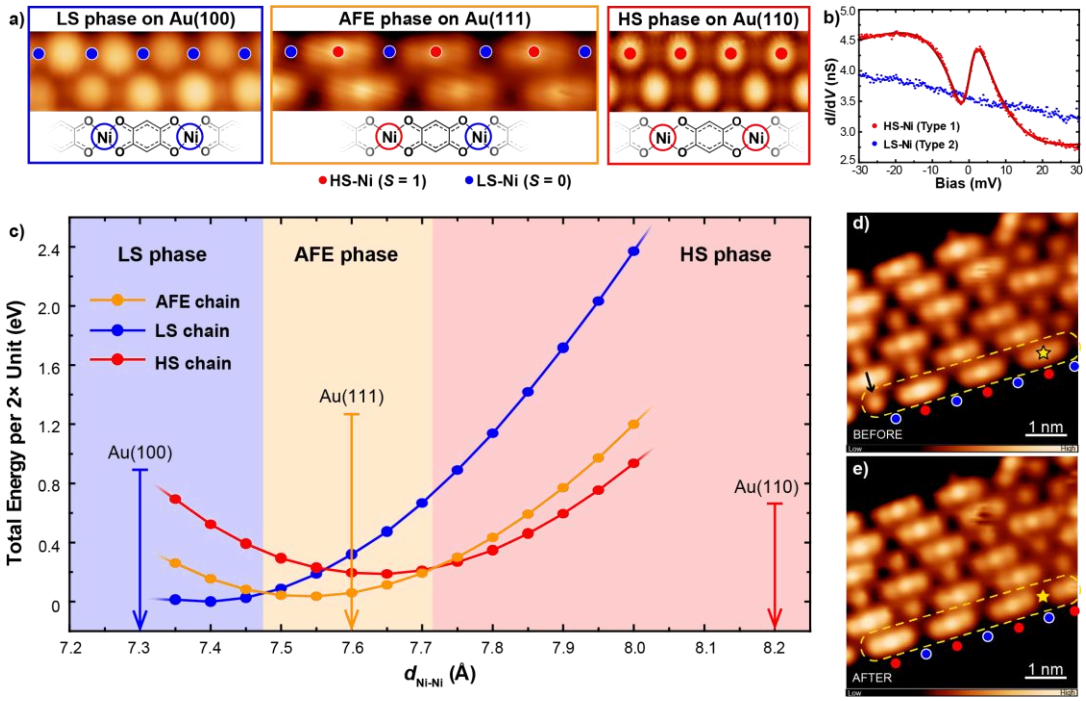

Figure 2. (a) STM images of the coordination chains formed by THB and Ni on Au(100) (left), Au(111) (middle), and Au(110) (right). (b) dI/dV curves acquired at the brighter (red) and darker (blue) Ni atoms in the chains on Au(111). (c) Spin-state phase diagram of the coordination chains. The Ni-Ni separations of the chains on the three Au surfaces are marked. STM images of the coordination chains on Au(111) (d) before and (e) after the tip-induced collective SCO switching. (a) and (c) are adapted with permission from Ref. 37. Copyright 2021 American

Chemical Society. (b) and (d) are adapted with permission from Ref. 36. Copyright 2020 American Chemical Society.

DFT calculations show that varying Ni-Ni separation in this 1D-cMOF structure leads to distinct ground states of the spin-state phase (Figure 2c) due to the magneto-structural effect of the Ni-O coordination nodes. The comparison of the chain periodicities and orientations with the substrate lattices reveals that the 1D chains commensurate with the substrate lattice on all the three Au surfaces. Therefore, the Ni-Ni separations in the chains are tuned by the substrate lattice and fall in the different regions of the phase diagram (Figure 2c), which results in the selective stabilization of different spin-state phases of the metal-organic chains on the three Au surfaces.

Specifically, a collective SCO in the 1D-cMOF chains prepared on Au(111) is demonstrated using tip excitations.[36] By applying voltage pulses, the brightness of multiple Ni atoms in the same coordination chain, which representing their spin states, are found to switch collectively (Figure 2d and e). Such collective conversions lead to the reversible switching between two degenerate states of the chain, that is, the transition between the spin-state configurations of "...101010..." and "...010101..." in the chain.

The realization of single-layer 2D-cMOFs by on-surface synthesis has been explored using benzene- or triphenylene-derived ligands with ortho-disubstituted N-, O-, or S-containing functional groups (Scheme 3a),[5,28,49,50] including metal-organic oligomers (Products 1 and 4 in Scheme 3b) *via* the coordination between 2,3,6,7,10,11-hexaaminotriphenylene (HATP, Scheme 3a) and Cu or Ni on Cu(111),[51] 2D thiolate coordination networks of $Ag_3(C_6S_6)$ (Product 4 in Scheme 3b), $Cu_6(C_6S_6)$ (Product 5 in Scheme 3b), and $Cu_8(C_6S_6)$ (Product 6 in Scheme 3b), on Ag(111) and Cu(111), using benzenehexathiol (BHT, Scheme 3a),[52] 2D networks with Ag_3 and Cu_3 clusters embedded (Product 2 in Scheme 3b) using hexahydroxytriphenylene (HHTP,

Scheme 3a) molecules on Ag(111) and Cu(111), respectively,[53] and extended 2D-cMOFs, of $Cu_3(C_6O_6)$ (Product 3 in Scheme 3b) on Cu(111)[54] and $Fe_3(C_6O_6)$ (Product 4 in Scheme 3b) on Au(111)[55] using benzenehexol (BHO, Scheme 3a), $Ni_3(HITP)_2$ (HITP: 2,3,6,7,10,11-hexaiminotriphenylene)[56] and $Fe_3(HITP)_2$[57] (both are Product 4 in Scheme 3b) on Au(111) using HATP. The combined STM and XPS studies in these works demonstrate the deprotonation of the molecular ligands, indicating that the deprotonated coordination reactions (Scheme 3b) are responsible for the formation of the metal-organic products on the surfaces.[51,52,54,55] Moreover, it's found in these studies that the careful control over the substrate-adlayer interactions and metal-organic interactions is crucial for the achievement of extended 2D metal-organic structures with high quality.[51,53]

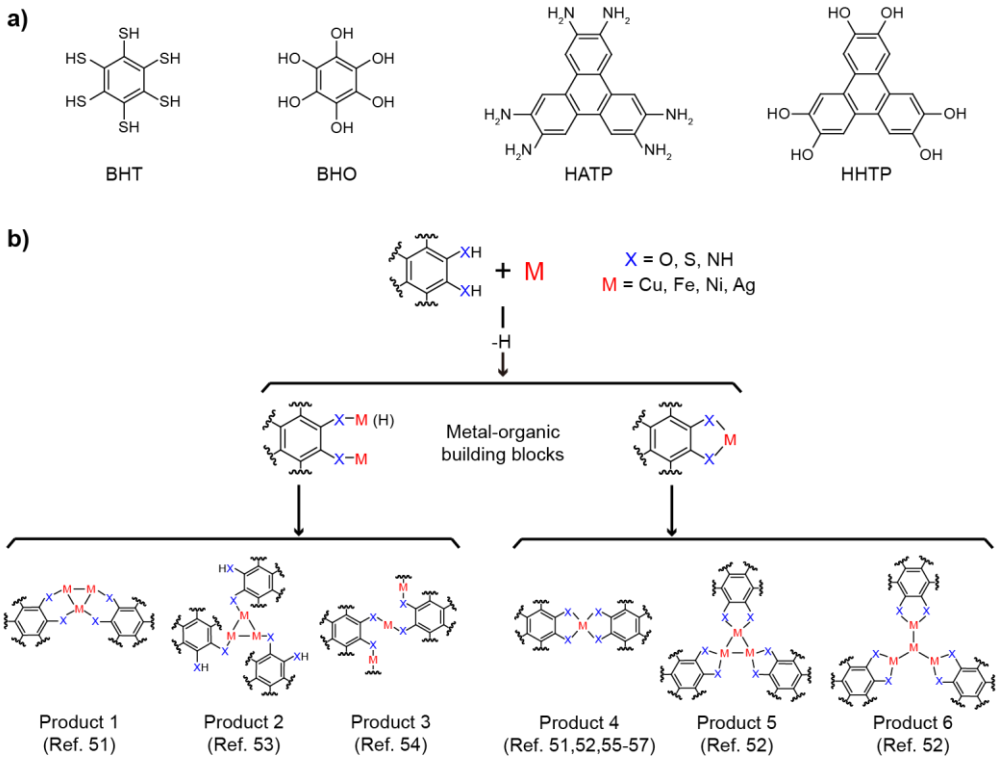

Scheme 3 (a) Chemical structures of the molecular ligands used for preparation of 2D-cMOFs on surfaces. (b) Schematic illustration of the on-surface dehydrogenation coordination reactions and the structure of the products proposed in the corresponding works.

A 2D-cMOF (Product 3 in Scheme 3b) is synthesized by the dehydrogenated coordination reaction between benzenehexol (BHO, Scheme 3a) and the Cu adatoms on Cu(111).[54] The STM topograph and DFT-optimized model of the $Cu_3(C_6O_6)$ monolayer are displayed in Figure 3a and b, respectively. Theoretical investigations reveal the band structures of the freestanding (Figure 3c) and surface adsorbed (Figure 3d) $Cu_3(C_6O_6)$, respectively. It can be clearly seen in Figure 3c that a highly dispersive band with a band width of 1 eV and an effective mass of 0.45 m_e appears above 2.7 eV. In addition, there are two narrow bands near the Fermi level, giving rise to a direct band gap at Γ point of 2.2 eV. Comparison between Figure 3c and d (the contribution from the MOF is drawn in thick black lines) shows that despite the down-shifted positions of the bands and the narrowed band gap of the absorbed $Cu_3(C_6O_6)$ monolayer, the main band characteristics of the freestanding structure, especially the dispersive conduction band, are preserved upon its adsorption on Cu(111). Further atom-specific analysis uncovers that the dispersive band is dominantly contributed by the d_{xy}, d_{z^2} and $d_{x^2-y^2}$ orbitals of Cu, and the $p_x + p_y$ orbitals of O. The coupling between these *d*, *p* orbitals with in-plane components results in a π-like nature of the conduction band and hence an in-plane conjugation of the O-Cu-O bonding motif. The latter was believed to be the origin of the dispersive conduction band. The theoretical results were confirmed by the experimental measurements. The power spectral map of $Cu_3(C_6O_6)$ (Figure 3e) enables direct observation of the dispersive conduction band above 0.8 V and the narrow bands at negative bias with a 1.5 V band gap between them. The larger experimental band gap in comparison with the calculated results was attributed to the underestimation of band gap in the DFT method.

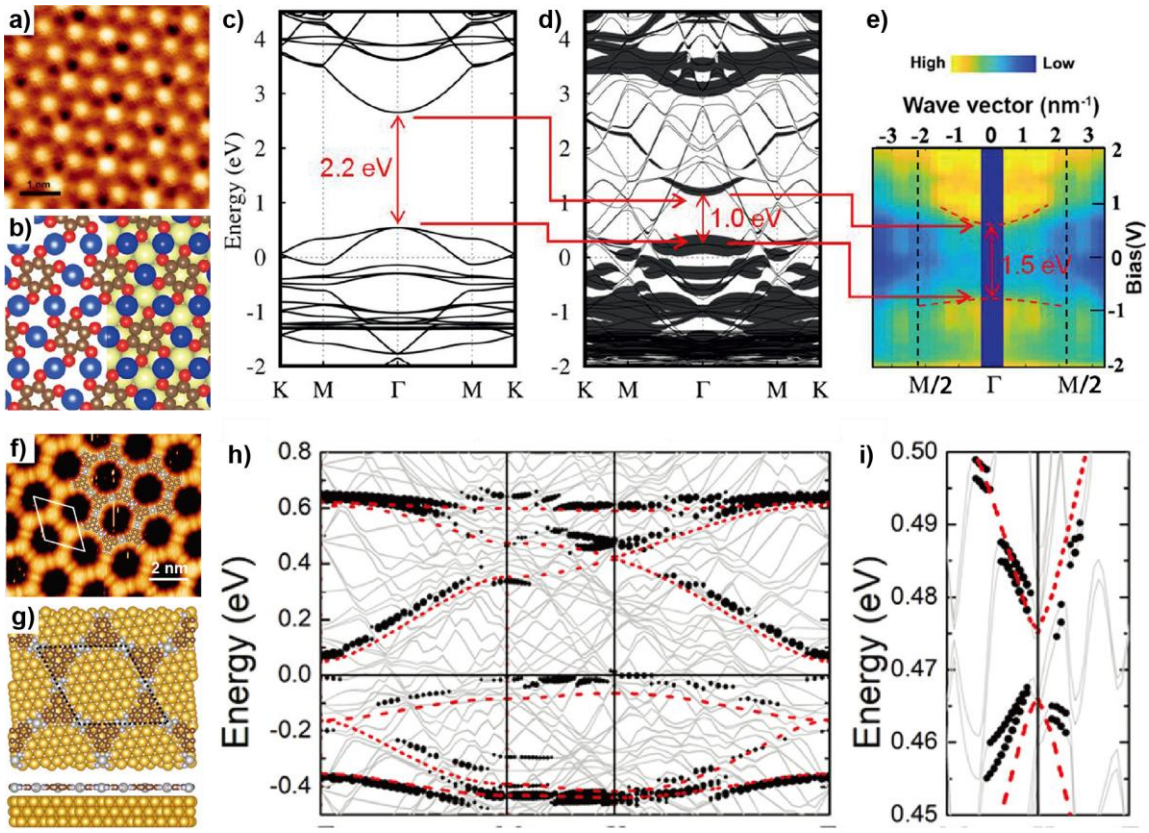

Figure 3 (a) STM image of $Cu_3(C_6O_6)$ on Cu(111). (b) Theoretically optimized model of the $Cu_3(C_6O_6)$ monolayer. Calculated electronic band structures of (c) the freestanding and (d) the absorbed $Cu_3(C_6O_6)$ monolayers. (e) Power-spectrum map acquired at a domain of $Cu_3(C_6O_6)$. Adapted with permission from Ref. 54. Copyright 2020 Wiley-VCH. (f) High-resolution STM image of the $Ni_3(HITP)_2$ monolayer on Au(111) with molecular models superimposed. (g) DFT optimized $Ni_3(HITP)_2$ monolayer on Au(111). (h) and (i) DFT-calculated band structures of the $Ni_3(HITP)_2$ monolayer absorbed on Au(111) with SOC. The contribution (>60%) of the $Ni_3(HITP)_2$ framework is highlighted by the black dotted lines. The bands of a free-standing $Ni_3(HITP)_2$ monolayer are up-shifted by 51 meV for comparison and marked by the red dotted lines. Adapted with permission from Ref. 56. Copyright 2021 Royal Society of Chemistry.

The dispersive bands were also found in the $Ni_3(HITP)_2$ monolayer on Au(111) achieved by the on-surface dehydrogenated coordination (Scheme 3b, Product 4) between HATP (Scheme 3a) and Ni.[56] $Ni_3(HITP)_2$ on Au(111) features a hexagonal framework comprising a Kagome lattice of Ni atoms (Figure 3f). The DFT-optimization of $Ni_3(HITP)_2$ on Au(111) (Figure 3g) yields a planar network with a relatively large Ni-substrate separation (3.460 Å) and a small adsorption energy (1.028 eV per unit cell), implying a weak monolayer-substrate interaction. The calculation of the electronic bands of $Ni_3(HITP)_2$ provides a direct comparison between the electronic structures of the freestanding (red dots in Figure 3c and d) and absorbed (black dots in Figure 3c and d) $Ni_3(HITP)_2$ monolayers. It's clearly seen in Figure 3h that the intrinsic band features of the freestanding $Ni_3(HITP)_2$ structure are largely preserved upon its adsorption on Au(111). Both the freestanding and absorbed $Ni_3(HITP)_2$ display highly dispersive bands, indicating their efficient conjugation. By taking SOC effect into consideration, a non-trivial gap of 8 meV is opened at the *K* point in the free-standing $Ni_3(HITP)_2$ framework (red dots in Figure 3i), and the gap is retained in the adsorbed monolayer (black dots in Figure 3i). These theoretical results provide evidence of a non-trivial topological gap in the absorbed $Ni_3(HITP)_2$ monolayer.

A series of extended 2D-MOFs exhibiting magnetic coupling were achieved by on-surface coordination chemistry.[68-72] Combined STM and X-ray magnetic circular dichroism (XMCD) investigations of these 2D-MOFs reveal either ferro- or antiferromagnetic interactions between the 3*d*-metal centers, which were ascribed to the super-exchange coupling *via* the molecular ligands.[69-71] In all these cases, conjugated organic ligands [*e.g.*, 7,7,8,8-tetracyanoquinodimethane,[68,70,71] 1,2,4,5-tetracyanobenzene,[72] and 2,4,6-tris(4-pyridyl)-1,3,5-triazine[69]] were used. It is in line with the theoretical study by Bellini *et al*.[67] concluding that efficient conjugation through the organic linkers in the metal-organic hybrids can enhance the

super-exchange coupling between the metal centers. In this context, 2D-cMOFs provide a playground for constructing various 2D magnetic orderings and exploring the related physics.

An example of the study addressing the magnetic coupling in an on-surface synthesized 2D-cMOF, $Fe_3(HITP)_2$.[57] Theoretical exploration of the freestanding $Fe_3(HITP)_2$ monolayer (Figure 4b) demonstrates a ferromagnetic ground state (Figure 4c) in which each Fe center possesses a net out-of-plane magnetic moment of 2.45 μ_B. The experimental realization of the single-layer $Fe_3(HITP)_2$ framework was achieved by dehydrogenated coordination (Scheme 3b, Product 4) of Fe and HATP (Scheme 3a) on Au(111). STM topograph of $Fe_3(HITP)_2$ on Au(111) (Figure 4a) shows a similar hexagonal framework with that of $Ni_3(HITP)_2$, in which the Fe atoms are arranged in a Kagome lattice, in agreement with the theoretical models. STS measurements show a V-shape feature around the Fermi level which can be attributed to either the Kondo effect or the spin excitations (Figure 4d). The dI/dV map at 8 mV provides a direct look at the spatial distribution of the V-shape resonance in the spectra. It can be seen in Figure 4e that the dim regions induced by the V-shape spectral feature are mainly localized at the Fe centers, which is consistent with the calculated spin density distribution, indicating the presence of a magnetic moment at the Kagome lattice of Fe atoms. In addition, the theoretical exploration also indicates this 2D-MOF structure as a promising candidate of a quantum anomalous Hall system

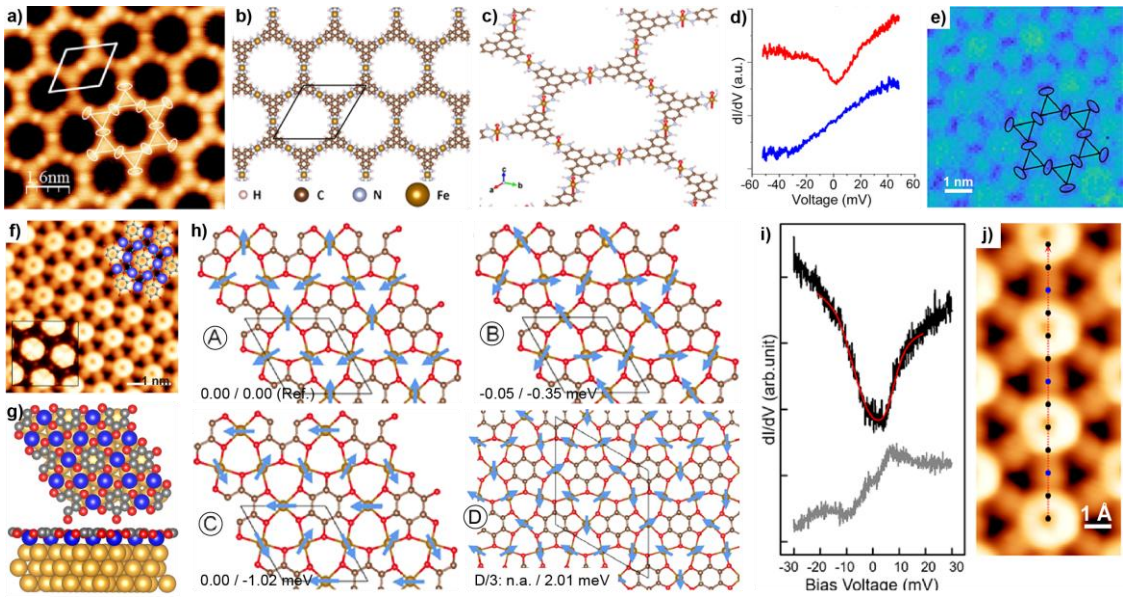

Figure 4 (a) High-resolution STM image of the single-layer $Fe_3(HITP)_2$ on Au(111). (b) DFT-optimized model of the free-standing $Fe_3(HITP)_2$ monolayer. (c) The out-of-plane ferromagnetic ground state of the freestanding $Fe_3(HITP)_2$ monolayer. (d) dI/dV spectra acquired at a Fe atom (red) and a molecular moiety (blue) near the Fermi level. (e) dI/dV map acquired at bias = 8 mV. Adapted with permission from Ref. 57. Copyright 2021 American Chemical Society. (f) High-resolution STM image of the $Fe_3(BHO_{-6H})$ monolayer on Au(111). Inset: STM image in constant-height mode. (g) DFT-optimized model of $Fe_3(BHO_{-6H})$ on Au(111). (h) DFT-calculated lowest-energy configurations of A, B, C, and D. The energy differences with respect to state A with/without substrate are marked at bottom-left of each configuration. (i) dI/dV spectra acquired at an Fe site (black) and the bare Au surface (grey). Spatially resolved dI/dV spectra are acquired along the dotted line in (j). Adapted with permission from Ref. 55. Copyright 2021 American Chemical Society.

A frustrated antiferromagnetic Kagome lattice is formed in a single-layer 2D-cMOF (Scheme 3b, Product 4) formed by BHO (Scheme 3a, denoting dehydrogenated BHO as BHO_{-6H} hereafter) and Fe on Au(111).[55] Combined STM, XPS and DFT investigations reveal a

stoichiometry of $Fe_3(BHO_{-6H})$ of the 2D framework which comprises a Kagome lattice of Fe atoms at a high-spin state of $S = 2$ (Figure 4f and g). In order to elucidate the magnetic ground state of the $Fe_3(BHO_{-6H})$ framework, the authors theoretically tested several magnetic configurations, including out-of-plane ferromagnetic, out-of-plane ferrimagnetic, in-plane ferrimagnetic, and in-plane antiferromagnetic. Consequently, it is found that the most energy-favorable configuration comprises the in-plane antiferromagnetically coupled Fe centers. Further calculations of several different in-plane antiferromagnetic configurations (Figure 4h), that is, A (also known as the $q = 0$ state of the Kagome lattice[73,74]), B, C and D (also known as the $q = \sqrt{3} \times \sqrt{3}$ state of the Kagome lattice[73,74]), uncover their comparable energies, suggesting them as degenerate ground states. A representative dI/dV spectrum shows two steps at ±6 mV (Figure 4i). The conductance steps were assigned to spin excitation caused by either magnetic anisotropy or a spin gap. The spatial resolved dI/dV spectra acquired along the dotted line in Figure 4j shows that the step feature associated with the spin excitation is a global effect taking place in the entire framework while appears stronger at the Fe atoms. This result likely indicates a spin gap as the origin of the spin excitation.

The concept of on-surface synthesis has been well demonstrated for designing and fabricating 1D- and 2D-cMOF structures. Though only being demonstrated in limited examples, this method already shows promising potentials to realize single-layer 1D- and 2D-cMOFs. Future developments of employing this method to fabricate free-standing single-layer 1D- and 2D-cMOFs or grow 1D- and 2D-cMOFs on decoupling layer are of great importance in order to investigate and harvest their intrinsic electronic and magnetic properties.

Acknowledgement: This work is supported financially by Hong Kong RGC 16301219.

References

1. Stavila, V.; Talin, A. A.; Allendorf, M. D. MOF-Based Electronic and Opto-Electronic Devices. *Chem. Soc. Rev.* **2014**, *43*, 5994-6010.
2. Zhu, L.; Liu, X. Q.; Jiang, H. L.; Sun, L. B. Metal-Organic Frameworks for Heterogeneous Basic Catalysis. *Chem. Rev.* **2017**, *117*, 8129-8176.
3. Kreno, L. E.; Leong, K.; Farha, O. K.; Allendorf, M.; Van Duyne, R. P.; Hupp, J. T. Metal-Organic Framework Materials as Chemical Sensors. *Chem. Rev.* **2012**, *112*, 1105-25.
4. Hendon, C. H.; Rieth, A. J.; Korzynski, M. D.; Dinca, M. Grand Challenges and Future Opportunities for Metal-Organic Frameworks. *ACS Cent. Sci.* **2017**, *3*, 554-563.
5. Sun, L.; Campbell, M. G.; Dincă, M. Electrically Conductive Porous Metal–Organic Frameworks. *Angew. Chem. Int. Ed.* **2016**, *55*, 3566-3579.
6. Kambe, T.; Sakamoto, R.; Hoshiko, K.; Takada, K.; Miyachi, M.; Ryu, J.-H.; Sasaki, S.; Kim, J.; Nakazato, K.; Takata, M.; et al. π-Conjugated Nickel Bis(dithiolene) Complex Nanosheet. *J. Am. Chem. Soc.* **2013**, *135*, 2462-2465.
7. Sakamoto, R.; Takada, K.; Pal, T.; Maeda, H.; Kambe, T.; Nishihara, H. Coordination Nanosheets (CONASHs): Strategies, Structures and Functions. *Chem. Commun.*, **2017**, *53*, 5781-5801.
8. Sheberla, D.; Sun, L.; Blood-Forsythe, M. A.; Er, S.; Wade, C. R.; Brozek, C. K.; Aspuru-Guzik, A.; Dincă, M. High Electrical Conductivity in Ni_3(2,3,6,7,10,11-hexaiminotriphenylene)$_2$, a Semiconducting Metal–Organic Graphene Analogue *J. Am. Chem. Soc.* **2014**, *136*, 8859-8862.
9. Huang, X.; Sheng, P.; Tu, Z.; Zhang, F.; Wang, J.; Geng, H.; Zou, Y.; Di, C.; Yi, Y.; Sun, Y.; Xu, W.; Zhu, D. A Two-Dimensional π–d Conjugated Coordination Polymer with Extremely High Electrical Conductivity and Ambipolar Transport Behaviour. *Nat. Commun.* **2015**, *6*, 7408.
10. Clough, A. J.; Skelton, J. M.; Downes, C. A.; de la Rosa, A. A.; Yoo, J. W.; Walsh, A.; Melot, B. C.; Marinescu, S. C. Metallic Conductivity in a Two-Dimensional Cobalt Dithiolene Metal–Organic Framework. *J. Am. Chem. Soc.* **2017**, *139*, 10863-10867.
11. Lahiri, N.; Lotfizadeh, N.; Tsuchikawa, R.; Deshpande, V. V.; Louie, J. Hexaaminobenzene as a Building Block for a Family of 2D Coordination Polymers. *J. Am. Chem. Soc.* **2016**, *139*, 19-22.
12. Campbell, M. G.; Sheberla, D.; Liu, S. F.; Swager, T. M.; Dincă, M. Cu_3(hexaiminotriphenylene)$_2$: An Electrically Conductive 2D Metal–Organic Framework for Chemiresistive Sensing. *Angew. Chem. Int. Ed.* **2015**, *54*, 4349-4352.
13. Kambe, T.; Sakamoto, R.; Kusamoto, T.; Pal, T.; Fukui, N.; Hoshiko, K.; Shimojima, T.; Wang, Z.; Hirahara, T.; Ishizaka, K.; et al. Redox Control and High Conductivity of Nickel Bis(dithiolene) Complex π-Nanosheet: A Potential Organic Two-Dimensional Topological Insulator. *J. Am. Chem. Soc.* **2014**, *136*, 14357-14360.
14. Pal, T.; Kambe, T.; Kusamoto, T.; Foo, M. L.; Matsuoka, R.; Sakamoto, R.; Nishiharam, H. Interfacial Synthesis of Electrically Conducting Palladium Bis(dithiolene) Complex

Nanosheet. *ChemPlusChem* **2015**, *80*, 1255-1258.

15. Wang, M.; Dong, R.; Feng X. *Chem. Soc. Rev.* **2021**, *50*, 2764-2793.
16. Zhang, X.; Zhou, Y.; Cui, B.; Zhao, M.; Liu, F. Theoretical Discovery of a Superconducting Two-Dimensional Metal−Organic Framework. *Nano Lett.* **2017**, *17*, 6166–6170
17. Huang, X.; Zhang, S.; Liu, L.; Yu, L.; Chen, G.; Xu, W.; Zhu, D. *Angew. Chem. Int. Ed.* **2018**, *57*, 146–150
18. Dong, R.; Zhang, Z.; Tranca, D. C.; Zhou, S.; Wang, M.; Adler, P.; Liao, Z.; Liu, F.; Sun, Y.; Shi, W.; et al. A Coronene-Based Semiconducting Two-Dimensional Metal-Organic Framework with Ferromagnetic Behavior. *Nat. Commun.* **2018**, *9*, 2637
19. Wang, Z. F.; Liu, Z.; Liu, F. Organic Topological Insulators in Organometallic Lattices. *Nat. Commun.* **2013**, *4*, 1471.
20. Liu, Z.; Wang, Z.-F.; Mei, J.-W.; Wu, Y.-S.; Liu, F. Flat Chern Band in a Two-Dimensional Organometallic Framework. *Phys. Rev. Lett.* **2013**, *110*, 106804.
21. Wang, Z. F.; Liu, Z.; Liu, F. Quantum Anomalous Hall Effect in 2D Organic Topological Insulators. *Phys. Rev. Lett.* **2013**, *110*, 196801.
22. Zhang, X.; Wang, Z.; Zhao, M.; Liu, F. Tunable Topological States in Electron-Doped HTT-Pt. *Phys. Rev. B.* **2016**, *93*, 165401.
23. Jiang, W.; Ni, X.; Liu, F. Exotic Topological Bands and Quantum States in Metal–Organic and Covalent–Organic Frameworks. *Acc. Chem. Res.* **2021**, *54*, 416-426.
24. Zhao, M.; Wang, A.; Zhang, X. Half-Metallicity of a Kagome Spin Lattice: The Case of a Manganese Bis-dithiolene Monolayer. *Nanoscale*, **2013**, *5*, 10404-10408.
25. Li, W.; Sun, L.; Qi, J.; Jarillo-Herrero, P.; Dinca, M.; Li, J. High Temperature Ferromagnetism in π-Conjugated Two-Dimensional Metal–Organic Frameworks. *Chem. Sci.* **2017**, *8*, 2859-2867.
26. Chen, S.; Dai, J.; Zeng, X. C. Metal–Organic Kagome Lattices M_3(2,3,6,7,10,11-hexaiminotriphenylene)$_2$ (M = Ni and Cu): From Semiconducting to Metallic by Metal Substitution. *Phys. Chem. Chem. Phys.* **2015**, *17*, 5954-5958.
27. Zhou, Q.; Wang, J.; Chwee, T. S.; Wu, G.; Wang, X.; Ye, Q.; Xu, J.; Yang, S.-W. Topological Insulators Based on 2D Shape-Persistent Organic Ligand Complexes. *Nanoscale* **2015**, *7*, 727-735.
28. Li, W.-H.; Deng, W.-H.; Wang, G.-E.; Xu, G. Conductive MOFs. *EnergyChem.* **2020**, *2*, 100029.
29. Dong, R.; Pfeffermann, M.; Liang, H.; Zheng, Z.; Zhu, X.; Zhang, J.; Feng, X. Large-Area, Free-Standing, Two-Dimensional Supramolecular Polymer Single-Layer Sheets for Highly Efficient Electrocatalytic Hydrogen Evolution. *Angew. Chem. Int. Ed.* **2015**, *54*, 12058-12063.
30. L. Dong, L.; Gao, Z. A.; Lin, N. Self-Assembly of Metal–Organic Coordination Structures on Surfaces. *Prog. Surf. Sci.* **2016**, *91*, 101-135.

31. Koudia, M.; Nardi, E.; Siri, O.; Abel, M. On-Surface Synthesis of Covalent Coordination Polymers on Micrometer Scale. *Nano Res.* **2017**, *10*, 933-940.

32. Denawi, H.; Koudia, M.; Hayn, R.; Siri, O.; Abel, M. On-Surface Synthesis of Spin Crossover Polymeric Chains. *J. Phys. Chem. C* **2018**, *122*, 15033-15040.

33. Denawi, H.; Nardi, E.; Koudia, M.; Siri, O.; Abel, M.; Hayn, R. Magnetic Polymer Chains of Iron and Zwitterionic Quinoidal Ligands on the Ag(111) Surface. *J. Phys. Chem. C* **2020**, *124*, 1346-1351.

34. Denawi, H.; Abel, M.; Hayn, R. Magnetic Polymer Chains of Transition Metal Atoms and Zwitterionic Quinone. *J. Phys. Chem. C* **2019**, *123*, 4582-4589.

35. Denawi, H.; Abel, M.; Siri, O.; Hayn, R. Electronic and Magnetic Properties of Metal-Organic Polymers with 4d and 5d-Transition Metal Ions. *J. Magn. Magn. Mater.* **2021**, *537*, 168183.

36. Liu, J.; Gao, Y. F.; Wang, T.; Xue, Q.; Hua, M. Q.; Wang, Y. F.; Huang, L.; Lin, N. Collective Spin Manipulation in Antiferroelastic Spin-Crossover Metallo-Supramolecular Chains. *ACS Nano* **2020**, *14*, 11283-11293.

37. Liu, J.; Li, J.; Chen, Q. W.; Xue, Q.; Wang, Y. F.; Di, B.; Wang, Y. F.; Wu, K. Lattice-Directed Stabilization of Different Spin-State Phases in Metallo-Supramolecular Chains on Au Surfaces. *Chem. Mater.* **2021**, *33*, 6166-6175.

38. Santhini, V. M.; Wäckerlin, C.; Cahlík, A.; Ondráček, M.; Pascal, S.; Matěj, A.; Stetsovych, O.; Mutombo, P.; Lazar, P.; Siri, O.; et al. 1D Coordination π-d Conjugated Polymers with Distinct Structures Defined by the Choice of the Transition Metal: Towards a New Class of Antiaromatic Macrocycles. *Angew. Chem. Int. Ed.* **2021**, *60*, 439-445.

39. Bose, S. Quantum Communication through an Unmodulated Spin Chain. *Phys. Rev. Lett.* **2003**, *91*, 207901.

40. Messina, P.; Dmitriev, A.; Lin, N.; Spillmann, H.; Abel, M.; Barth, J. V.; Kern, K. Direct Observation of Chiral Metal-Organic Complexes Assembled on a Cu(100) Surface. *J. Am. Chem. Soc.* **2002**, *124*, 14000-14001.

41. Lin, N.; Dmitriev, A.; Weckesser, J.; Barth, J. V.; Kern, K. Real-Time Single-Molecule Imaging of the Formation and Dynamics of Coordination Compounds. *Angew. Chem. Int. Ed.* **2002**, *41*, 4779-4783.

42. Kezilebieke, S.; Amokrane, A.; Abel, M.; Bucher, J.-P. Hierarchy of Chemical Bonding in the Synthesis of Fe-Phthalocyanine on Metal Surfaces: A Local Spectroscopy Approach. *J. Phys. Chem. Lett.* **2014**, *5*, 3175-3182.

43. Kezilebieke, S.; Amokrane, A.; Boero, M.; Clair, S.; Abel, M.; Bucher, J.-P. Steric and Electronic Selectivity in the Synthesis of Fe-1,2,4,5-Tetracyanobenzene (TCNB) Complexes on Au(111): From Topological Confinement to Bond Formation. *Nano Res.* **2014**, *7*, 888-897.

44. Koudia, M.; Abel, M. Step-by-Step on-Surface Synthesis: From Manganese Phthalocyanines to Their Polymeric Form. *Chem. Commun.* **2014**, *50*, 8565-8567.

45. Sakamoto, R.; Takada, K.; Sun, X.; Pal, T.; Tsukamoto, T.; Phua, E. J. H.; Rapakousiou, A.; Hoshiko, K.; Nishihara, H. The Coordination Nanosheet (CONASH). *Coord. Chem. Rev.* **2016**, *320*, 118-128.

46. Kambe, T.; Sakamoto, R.; Hoshiko, K.; Takada, K.; Miyachi, M.; Ryu, J.-H.; Sasaki, S.; Kim, J.; Nakazato, K.; Takata, M.; et al. π-Conjugated Nickel Bis(Dithiolene) Complex Nanosheet. *J. Am. Chem. Soc.* **2013**, *135*, 2462-2465.

47. Nardi, E.; Chen, L.; Clair, S.; Koudia, M.; Giovanelli, L.; Feng, X. L.; Mullen, K.; Abel, M. On-Surface Reaction between Tetracarbonitrile-Functionalized Molecules and Copper Atoms. *J. Phys. Chem. C* **2014**, *118*, 27549-27553.

48. Hauser, A. Ligand Field Theoretical Considerations. *Top. Curr. Chem.* **2004**, *233*, 49-58.

49. Maeda, H.; Sakamoto, R.; Nishihara, H. Coordination Programming of Two-Dimensional Metal Complex Frameworks. *Langmuir* **2016**, *32*, 2527-2538.

50. Ko, M.; Mendecki, L.; Mirica, K. A. Conductive Two-Dimensional Metal-Organic Frameworks as Multifunctional Materials. *Chem. Commun.* **2018**, *54*, 7873-7891.

51. Lischka, M.; Dong, R.; Wang, M.; Martsinovich, N.; Fritton, M.; Grossmann, L.; Heckl, W. M.; Feng, X.; Lackinger, M. Competitive Metal Coordination of Hexaaminotriphenylene on Cu(111) by Intrinsic Copper Versus Extrinsic Nickel Adatoms. *Chem. Eur. J.* **2019**, *25*, 1975-1983.

52. Meng, X.; Kolodzeiski, E.; Huang, X.; Timmer, A.; Schulze Lammers, B.; Gao, H. Y.; Mönig, H.; Liu, L.; Xu, W.; Amirjalayer, S.; et al. Tunable Thiolate Coordination Networks on Metal Surfaces. *ChemNanoMat* **2020**, *6*, 1479-1484.

53. Rochefort, A.; Vernisse, L.; Gómez-Herrero, A. C.; Sánchez-Sánchez, C.; Martín-Gago, J. A.; Chérioux, F.; Clair, S.; Coraux, J.; Martínez, J. I. Role of the Structure and Reactivity of Cu and Ag Surfaces in the Formation of a 2D Metal–Hexahydroxytriphenylene Network. *J. Phys. Chem. C* **2021**, *125*, 17333-17341.

54. Zhang, R.; Liu, J.; Gao, Y.; Hua, M.; Xia, B.; Knecht, P.; Papageorgiou, A. C.; Reichert, J.; Barth, J. V.; Xu, H.; et al. On-Surface Synthesis of a Semiconducting 2D Metal-Organic Framework $Cu_3(C_6O_6)$ Exhibiting Dispersive Electronic Bands. *Angew. Chem. Int. Ed.* **2020**, *59*, 2669-2673.

55. Hua, M.; Xia, B.; Wang, M.; Li, E.; Liu, J.; Wu, T.; Wang, Y.; Li, R.; Ding, H.; Hu, J.; et al. Highly Degenerate Ground States in a Frustrated Antiferromagnetic Kagome Lattice in a Two-Dimensional Metal-Organic Framework. *J. Phys. Chem. Lett.* **2021**, *12*, 3733-3739.

56. Gao, Z.; Hsu, C. H.; Liu, J.; Chuang, F. C.; Zhang, R.; Xia, B.; Xu, H.; Huang, L.; Jin, Q.; Liu, P. N.; et al. Synthesis and Characterization of a Single-Layer Conjugated Metal-Organic Structure Featuring a Non-Trivial Topological Gap. *Nanoscale* **2019**, *11*, 878-881.

57. Gao, Z. A.; Gao, Y.; Hua, M.; Liu, J.; Huang, L.; Lin, N. Design and Synthesis of a Single-Layer Ferromagnetic Metal–Organic Framework with Topological Nontrivial Gaps. *J. Phys. Chem. C* **2020**, *124*, 27017-27023.

58. Weber-Bargioni, A.; Reichert, J.; Seitsonen, A. P.; Auwa, W.; Barth, J. V. Interaction of Cerium Atoms with Surface-Anchored Porphyrin Molecules. *J. Phys. Chem. Lett.* **2008**, *112*, 3453-3455.

59. Liljeroth, P.; Swart, I.; Paavilainen, S.; Repp, J.; Meyer, G. Single-Molecule Synthesis and Characterization of Metal-Ligand Complexes by Low-Temperature Stm. *Nano. Lett.* **2010**, *10*, 2475-2479.

60. Mohn, F.; Repp, J.; Gross, L.; Meyer, G.; Dyer, M. S.; Persson, M. Reversible Bond Formation in a Gold-Atom-Organic-Molecule Complex as a Molecular Switch. *Phys. Rev. Lett.* **2010**, *105*, 266102.

61. Ohmann, R.; Vitali, L.; Kern, K. Actuated Transitory Metal-Ligand Bond as Tunable Electromechanical Switch. *Nano Lett.* **2010**, *10*, 2995-3000.

62. Wang, W.; Hong, Y.; Shi, X.; Minot, C.; Hove, M. A. V.; Tang, B. Z.; Lin, N. Inspecting Metal-Coordination-Induced Perturbation of Molecular Ligand Orbitals at a Submolecular Resolution. *J. Phys. Chem. Lett.* **2010**, *1*, 2295-2298.

63. Wang, W.; Shi, X.; Lin, C.; Zhang, R. Q.; Minot, C.; Van Hove, M. A.; Hong, Y.; Tang, B. Z.; Lin, N. Manipulating Localized Molecular Orbitals by Single-Atom Contacts. *Phys. Rev. Lett.* **2010**, *105*, 126801.

64. Wang, W.; Shi, X.; Wang, S.; Liu, J.; Van Hove, M. A.; Liu, P. N.; Zhang, R. Q.; Lin, N. Cooperative Modulation of Electronic Structures of Aromatic Molecules Coupled to Multiple Metal Contacts. *Phys. Rev. Lett.* **2013**, *110*, 046802.

65. Gambardella, P.; Stepanow, S.; Dmitriev, A.; Honolka, J.; de Groot, F. M.; Lingenfelder, M.; Sen Gupta, S.; Sarma, D. D.; Bencok, P.; Stanescu, S.; et al. Supramolecular Control of the Magnetic Anisotropy in Two-Dimensional High-Spin Fe Arrays at a Metal Interface. *Nat. Mater.* **2009**, *8*, 189-193.

66. Wegner, D.; Yamachika, R.; Zhang, X.; Wang, Y.; Baruah, T.; Pederson, M. R.; Bartlett, B. M.; Long, J. R.; Crommie, M. F. Tuning Molecule-Mediated Spin Coupling in Bottom-up-Fabricated Vanadium-Tetracyanoethylene Nanostructures. *Phys. Rev. Lett.* **2009**, *103*, 087205.

67. Bellini, V.; Lorusso, G.; Candini, A.; Wernsdorfer, W.; Faust, T. B.; Timco, G. A.; Winpenny, R. E.; Affronte, M. Propagation of Spin Information at the Supramolecular Scale through Heteroaromatic Linkers. *Phys. Rev. Lett.* **2011**, *106*, 227205.

68. Tseng, T.-C.; Lin, C.; Shi, X.; Tait, S.; Liu, X.; Starke, U.; Lin, N.; Zhang, R.; Minot, C.; Van Hove, M.; et al. Two-Dimensional Metal-Organic Coordination Networks of Mn-7,7,8,8-Tetracyanoquinodimethane Assembled on Cu(100): Structural, Electronic, and Magnetic Properties. *Phys. Rev. B* **2009**, *80*, 155458.

69. Umbach, T. R.; Bernien, M.; Hermanns, C. F.; Kruger, A.; Sessi, V.; Fernandez-Torrente, I.; Stoll, P.; Pascual, J. I.; Franke, K. J.; Kuch, W. Ferromagnetic Coupling of Mononuclear Fe Centers in a Self-Assembled Metal-Organic Network on Au(111). *Phys. Rev. Lett.* **2012**, *109*, 267207.

70. Abdurakhmanova, N.; Tseng, T. C.; Langner, A.; Kley, C. S.; Sessi, V.; Stepanow, S.; Kern, K. Superexchange-Mediated Ferromagnetic Coupling in Two-Dimensional Ni-TCNQ Networks on Metal Surfaces. *Phys. Rev. Lett.* **2013**, *110*, 027202.

71. Faraggi, M. N.; Golovach, V. N.; Stepanow, S.; Tseng, T.-C.; Abdurakhmanova, N.; Kley, C. S.; Langner, A.; Sessi, V.; Kern, K.; Arnau, A. Modeling Ferro- and Antiferromagnetic

Interactions in Metal–Organic Coordination Networks. *J. Phys. Chem. C* **2014**, *119*, 547-555.

72. Giovanelli, L.; Savoyant, A.; Abel, M.; Maccherozzi, F.; Ksari, Y.; Koudia, M.; Hayn, R.; Choueikani, F.; Otero, E.; Ohresser, P.; et al. Magnetic Coupling and Single-Ion Anisotropy in Surface-Supported Mn-Based Metal–Organic Networks. *J. Phys. Chem. C* **2014**, *118*, 11738-11744.
73. Grohol, D.; Matan, K.; Cho, J. H.; Lee, S. H.; Lynn, J. W.; Nocera, D. G.; Lee, Y. S. Spin Chirality on a Two-Dimensional Frustrated Lattice. *Nat. Mater.* **2005**, *4*, 323-328.
74. Chernyshev, A. L.; Zhitomirsky, M. E. Quantum Selection of Order in an XXZ Antiferromagnet on a Kagome Lattice. *Phys. Rev. Lett.* **2014**, *113*, 237202.